Materials Horizons

ROYAL SOCIETY OF CHEMISTRY

COMMUNICATION

View Article Online
View Journal | View Issue

Check for updates

Cite this: *Mater. Horiz.*, 2024, 11, 5768

Received 13th June 2024,
Accepted 2nd September 2024

DOI: 10.1039/d4mh00755g

rsc.li/materials-horizons

Rapid spread, slow evaporation: a long-lasting water film on hydrogel nanowire arrays for continuous wearables†

Peijia Li,[ad] Yilin Wang,[ad] Ming Qiu,[a] Yixiao Wang,[a] Zhaoxiang Lu,[b] Jianning Yu,[a] Fan Xia,[c] Yun Feng*[b] and Ye Tian*[ade]

A successful flexible wearable not only has to fulfill its function, but also has to ensure long-term wettability and comfort during wearing. In biological systems, tears spread rapidly across the cornea to ensure clear imaging while slowly evaporating to maintain moisture in the eyes. This dynamic behavior of 'rapid spread, slow evaporation' ensures durative humidity and comfort, which can provide design guidelines for continuous wearable devices. However, realizing this dynamic process *in vitro* remains a challenge. Herein, inspired by a healthy ocular surface, we biomimetically construct a hybrid surface featuring mucin-like hydrophilic layer@hydrogel nanowire arrays (HL@HNWs). A droplet (2 μL) rapidly spreads into a thin film, stabilizing for ~10 minutes, whereas the contrast sample rapidly ruptures and dewets within 1 minute. We demonstrate that enhancing the proportion of hydrated water (HW), which includes intermediate water (IW) and bound water (BW), and introducing the capillary resistance of the nanowire arrays could synergistically stabilize the water film and improve the wettability. Hydrogel-based nanowire array contact lenses can ensure wettability during continuous wear, and a stable water film can substantially improve comfort and provide superior visual quality.

New concepts

Hydrogel-based flexible wearable devices have been widely used in personalized healthcare. However, practical applications of hydrogels may involve variable hydration environments, and the inevitable evaporation of water leads to discomfort during continuous wear. The dynamic behaviour of 'rapid spread, slow evaporation' of a healthy tear film ensures durative humidity and comfort, which can provide design guidelines for continuously wearable hydrogel-based devices. Here, a novel wearable device with enhanced long-term hydration stability is demonstrated by *in vitro* assembly of an ocular-like surface in combination with nanowire arrays and strong hydration layers. This strategy of combining nanowire arrays and a molecular level hydration layer leads to water film stability improvement and continuous wear comfort. Therefore, the obtained hydrogel eye contact device can significantly optimize long-term wettability and visual quality. This material design concept will have a wide range of applications, which can usher in an alternative paradigm to enhance wearable comfort for other hydrogel-based wearable devices.

1. Introduction

With the growing demand for personalized healthcare, hydrogel-based flexible wearable systems have received great attention.[1–3] Hydrogels with excellent biocompatibility and mechanical features close to those of human tissues constitute a promising approach for realizing healthcare-oriented functionalities.[4–6] However, practical applications of wearables may involve significantly varying thermal and hydrated environments, leading to discomfort during long-term use due to the inevitable evaporation of water in dehydrated conditions.[7] Furthermore, in dry environments, the interfacial adhesion may be weakened by the occurrence of water at the device-air interface, which can result in potential device delamination.[8,9] Thus, the challenge remains in how to fulfil a wearable's function and adapt to complex environments while ensuring comfort during wear.

In biological systems, tears can quickly spread on the healthy cornea surface, forming an ultrathin liquid film. This

[a] *Laboratory of Bio-Inspired Materials and Interface Sciences, Technical Institute of Physics and Chemistry, Chinese Academy of Sciences, Beijing 100190, China. E-mail: tianyely@iccas.ac.cn*
[b] *Department of Ophthalmology, Peking University Third Hospital, Beijing 100191, China. E-mail: fengyun@bjmu.edu.cn*
[c] *State Key Laboratory of Biogeology and Environmental Geology, Faculty of Materials Science and Chemistry, China University of Geosciences, Wuhan 430078, China*
[d] *School of Future Technology, University of Chinese Academy of Sciences, Beijing 100049, China*
[e] *Suzhou Institute for Advanced Research, University of Science and Technology of China, Jiangsu 215123, China*

† Electronic supplementary information (ESI) available. See DOI: https://doi.org/10.1039/d4mh00755g

film undergoes slow evaporation to maintain stability during the next blink. The dynamic behaviour of 'rapid spread and slow evaporation' of tears on the corneal surface is vital for maintaining eye surface comfort, ensuring clear vision and keeping eyes lubricated.[10,11] This dynamic behaviour of 'rapid spread, slow evaporation' ensures durable humidity and comfort, which can provide design guidelines for continuous hydrogel-based wearable devices.

The stability of healthy biological tear films relies primarily on the intricate tear microenvironment.[12] Specifically, membrane-associated mucins with polysaccharide carboxyl residues attached to microvilli arrays play a significant role.[13,14] They not only provide a hydrophilic base for the even spread of tear film but also synergically strengthen the anchoring effect of tears on the ocular surface. This prevents premature tear-film dewetting and breakup, ensuring continuous coverage and wettability of the eye surface.[15] Some studies have been effective in maintaining the wetness and comfort of lenses. For example, Zhu *et al.* reported a microfluidic hydrogel blinking system with integrated microchannels to prevent dry eyes and discomfort by blinking to assist tear flow.[16] Kusama *et al.* reported that electroosmotic flow can be induced in a soft contact lens to maintain the moisture of the lens.[17] More recently, self-lubricating lenses have been prepared by injecting lubricants into the lens surface to maintain lasting wettability.[18] These methods effectively maintain the wetness and comfort of the lens, but require complex processing and periodic updates to maintain lens moisture, which makes it difficult to commercialize.

Herein, inspired by the healthy cornea surface, we construct a hybrid surface comprising a mucin-like hydrophilic layer atop silicon-based hydrogel nanowire arrays. On this surface, a 2 μL droplet quickly spreads into a thin liquid film and maintains its stability for ~10 minutes at the air–liquid interface. In contrast, on surfaces lacking this hybrid composition, droplets would rapidly rupture and dewet within 1 minute. Macroscopic observations of water film stabilization phenomena, along with microscopic characterizations of the interfacial water structure, demonstrate that the stability is attributed to the synergistic effect between the capillary resistance of the nanowire arrays and the higher ratio of hydrated water (HW), which includes intermediate water (IW) and bound water (BW). Specifically, the nanowire arrays serve as crucial initiators for liquid film stabilization. Further, the presence of more HWs and lower mobility of water molecules contribute to a more stable water film. These gel-based continuous wearable contact lens can substantially improve comfort and provide superior visual quality and long-term moisturizing. In addition, this design concept can be expected to be applied to various wearable devices to obtain multi-functional integrated wearable devices with comfort, high hydrophilicity and high humidity.[3,19]

2. Results and discussion

Fabrication of TE@HNWs

The ingenious composition of the cornea is essential for tear film stabilization, in which a hydrophilic mucin layer is anchored onto hydrophobic epithelium nanowire arrays (Fig. 1a and Fig. S1 (ESI†), healthy area zoomed in to the right). To mimic the microstructure of the cornea, a bioinspired hydrogel nanowire array is fabricated by the replica molding method, which is further modified with a carboxylate coating (Fig. 1b). For a typical fabrication process, a mixture of silicone monomer 3-(methacryloyloxypropyl) tris(trimethylsiloxy)silane (SiM), *N*-vinylpyrrolidone (NVP) and 2-hydroxyethyl methacrylate (HEMA) (Fig. 1c, left panel) is illuminated under a lamp within porous anodic aluminum oxide (AAO) templates. After polymerization, $CuCl_2$ and NaOH solutions are used in turn to dissolve the AAO templates, and various lengths of silane-based hydrogel nanowires (HNWs) can be obtained by changing the thickness of the AAO templates.[20] To graft a covalently anchored carboxylate layer on the samples, the HNWs are oxidized by air plasma and then treated with a mixed solution (V_{H_2O} : V_{HCl} : $V_{H_2O_2}$, 5 : 1 : 1) to generate abundant surface hydroxyl groups (–OH) (Fig. S2, ESI†). Afterward, the HNWs are incubated in solutions of a coupling agent of *N*-[(3-trimethoxysilyl)propyl]-ethylenediamine triacetic acid trisodium salt (abbreviated as TE) at 50 °C for 5 h (Fig. 1c, right panel).[21,22] Finally, the TE macromolecules are covalently grafted onto the HNWs through a coupling reaction between Si–O–R and –OH, the product being named as TE@HNWs.

Uniformly dispersed nanowire arrays are clearly observed from both the surface and cross-sectional SEM images of the HNWs and TE@HNWs with a length of 3 μm (Fig. 1d). In contrast, varying degrees of aggregation or collapse occur on shorter and longer nanowire array surfaces (Fig. S3, ESI†). A dispersed and vertical nanowire array structure is essential for the capillary effect generation. Hence in order to get an in-depth insight into the functionality of the nanowire arrays, the tests described in the following are performed on 3 μm nanowire arrays except where noted otherwise. Additionally, attenuated total reflectance Fourier transform infrared spectroscopy (ATR-FTIR) characterization of HNWs detects a wide band at 3000 cm^{-1} and a sharp peak at 1650 cm^{-1}, corresponding to the existence of carboxyl groups (Fig. S4, ESI†).[23] Furthermore, a water droplet superspreads to CAs of ≈0° on the TE@HNWs surface. And even if the surface is exposed to air environment for a day, the property of superspreading can be recovered after immersing in water for several hours (Fig. 1e, bottom panel). This indicates that the hybrid structure is robust. Additionally, the TE@HNWs hardly deform or lose transparency during exposure. In summary, we obtain a stable bionic corneal surface, and for which the effect of the nanowire arrays and hydrophilic layer on the stability of the water film could be studied in depth.

Spreading process and water film stability

In order to understand the role of nanowire arrays and mucin-like TE hydrophilic layers in the superspreading process and water film stability process, dynamic spreading processes are investigated with *in situ* microscopy observations of water film variation on hydrogels with different grafting concentrations, including 0.5% TE@HNWs, 0.1% TE@HNWs, 0.5% TE@flat,

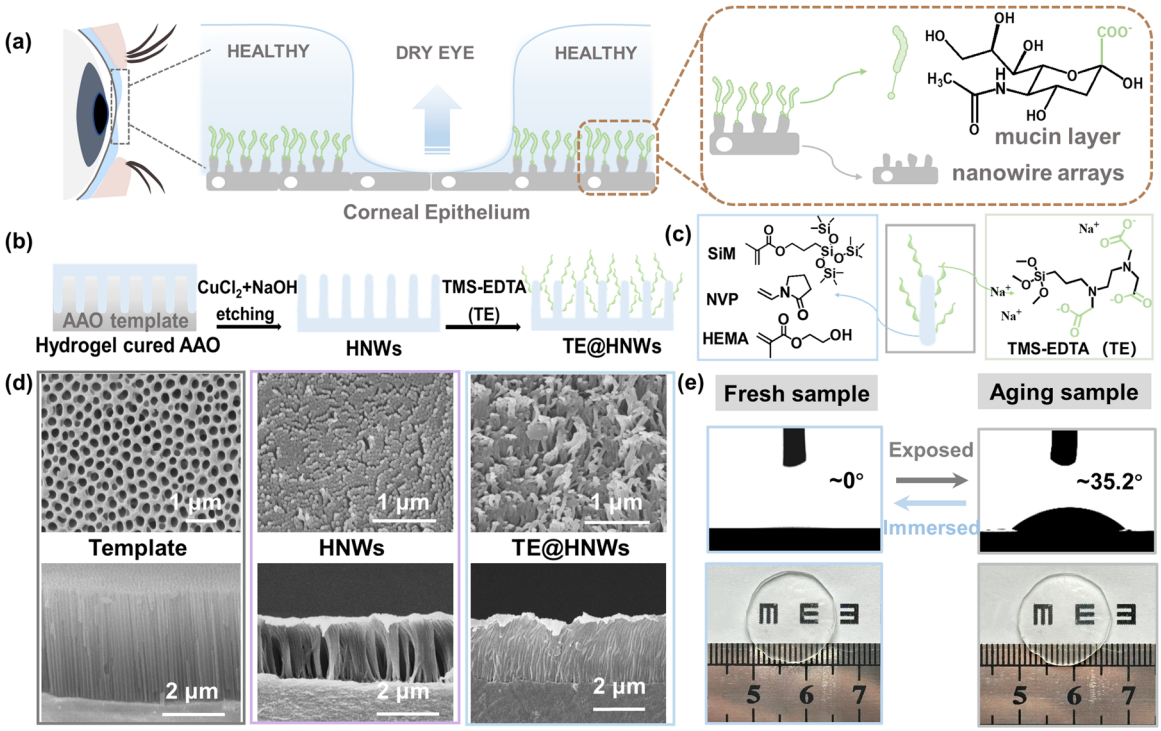

Fig. 1 Construction of a hybrid surface comprising mucin-like@silicon-based hydrogel nanowire arrays. (a) Schematic representation of tear film on the cornea suffering from dry eye disease. The two ingenious factors of tear film on the healthy cornea are zoomed in the right-hand panel, *i.e.*, nanowire arrays and a mucin layer with abundant carboxyl groups. (b) Fabrication process of TE@HNWs. The hydrogel nanowire arrays (HNWs) are obtained by the replica molding method, which are then covalently grafted with a carboxylate layer (TE@HNWs). (c) The chemical structure of monomers and carboxylate coupling reagent used to prepare the TE@HNWs. (d) SEM images of template (left), HNWs (middle) and TE@HNWs (right) from a top view and a side view. (e) Exposed to air environment for a day, the TE@HNWs keep their initial shape and high transparency. And the property of superspreading can be recovered after immersing in water for several hours.

and 0.1% TE@flat surfaces. The degree of ionization of the carboxyl group is different under different pHs, and the wetting characteristics are strongly related to the surface charge density. The 0.1% TE@HNWs surface (Fig. S5, ESI†) has the highest surface charge density at pH 9, which induces the fastest superspreading rate of a water droplet (volume of 2 μL) compared to other pHs. Therefore, pH 9 is determined as the optimum pH value for the subsequent tests. In detail, we first observe the spreading process on TE@HNWs with 3 μm nanowires arrays. We find that a water droplet can superspread to a CA of 0° within 2.46 s on 0.5% TE@HNWs (Fig. 2a, left panel), while it takes 2.72 s on 0.1% TE@HNWs surface (Fig. 2a, right panel). In comparison, the spreading performance is hindered due to insufficient capillary effect on 0.5% TE@HNWs with 1, 2, and 4 μm nanowire arrays (Fig. S7, ESI†). For comparison, a water droplet of the same volume is unable to superspread on the TE@flat surface regardless of grafting concentration (Fig. 2b). These studies indicate that the hydrophilic layer is capable of anchoring onto the low-energy surfaces, providing a hydrophilic base for the hydrophobic nanowire arrays to promote superspreading. More importantly, it is difficult for the hydrophilic TE layer to lower the surface energy of the flat surface to achieve superspreading behavior, suggesting that the capillary effect of the nanowire arrays is indispensable.

We then use *in situ* microscopy to investigate the stability of a thin water film fronts (≤10 μm) on different hydrogel surfaces. What is clearly observed is that the edge of the water film on 0.5% TE@HNWs (Fig. 2c, left panel) remains intact and without any rupture or unstable vibration for 5 minutes or even longer (Fig. S8a, ESI†), and the initial liquid film boundary remains pinned without receding. Nevertheless, at the same grafting concentration (0.5% TE@HNWs), the water film is premature and exhibits unstable fluctuations on nanowire arrays of other lengths within 1 min (Fig. S8b and c, ESI†). Subsequently, decreasing the grafting concentration to 0.1%, the stability of the water film weakened. The water film is intact within 1 min, but is severely loosened at 5 min (Fig. 2c, right panel). However, the water film on 0.5% TE@flat rapidly ruptures within 1 minute and generates unstable diffraction stripes, which disappear from view completely within 5 minutes (Fig. 2d, left panel). On decreasing the grafting concentration of TE to 0.1% (Fig. 2d, right panel), the stability of the water film becomes significantly worse. In order to quantify the change of water film macroscopically, the mass change of water droplets on the surface is monitored in real time with an analytical balance (Fig. S10, ESI†). Obviously, the speed of water loss on the 0.5% TE@flat surface is 1.5 times that on the 0.5% TE@HNWs surface. These comparative results

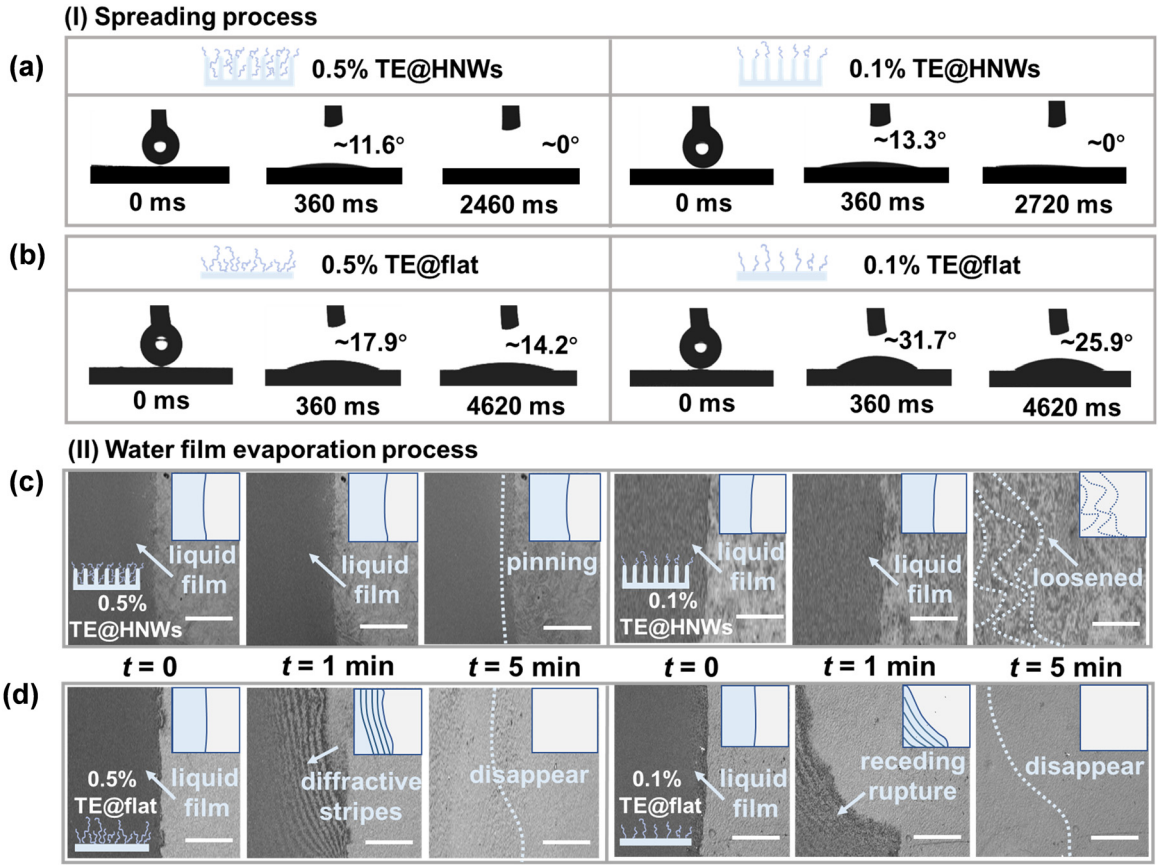

Fig. 2 The performance of (I) spreading processes and (II) water film evaporation process on different hydrogel surfaces. (I) Spreading process: CA snapshots of a water droplet (2 μL) on (a) TE@HNWs and (b) TE@flat surfaces of different TE concentration. The water droplet can superspread on the TE@HNWs surface, while being hydrophilic on the TE@flat surface. (II) Water film evaporation process on different hydrogel surfaces: optical images of the edge of water film at different times on (c) TE@HNWs and (d) TE@flat surface. The water film maintains longer-term stability on the TE@HNWs but ruptures early on the TE@flat surface. The scale bar is 200 μm.

demonstrate that the water film stability is engendered by the capillary resistance of the nanowire arrays and which is reinforced by the hydrophilic TE layer. In summary, both the droplet spreading process and water film stability process are inseparable from the synergistic mechanism of capillary effect of the nanowire arrays and hydration of the hydrophilic layer. Meanwhile, it is confirmed that the structure of nano-villi on the cornea and mucin components in tears are very important for tear superspreading and stability maintenance, which can provide a theoretical basis for the etiology of clinical dry eye disease.

Hydrated water distribution on different hydrogel surfaces

Many functionalities of surfaces can be directly correlated to specific types of interfacial water molecules, *e.g.*, the phase change behavior of water is strongly dependent on activated weakly bound water.[24–26] Therefore, it is highly desirable to elucidate the effect of interfacial hydrated water molecules on water film stability on hydrogel surfaces. According to the difference of intermolecular hydrogen bonding, the water in a hydrated hydrogel network has been classified into three types (Fig. 3a): free water (FW), intermediate water (IW), and bound water (BW).[27] Different types of hydrated water distribution could correspond to water film variation.

We analyze ATR-FTIR spectra in the region of O–H stretching to show the difference in hydrogen bonding of water molecules, revealing the water state in different hydrogel surfaces (see details in Fig. 3b). The peaks at ~3100 and 3250 cm^{-1} correspond to non-hydrated water (NHW), which is FW with four hydrogen bonds (Fig. 3b, orange and purple curves), while the peaks at ~3414 and 3514 cm^{-1} are associated with hydrated water (HW) in which the weakly or non-hydrogen bonded water molecules have been partially or entirely broken by polymer chains, *i.e.*, BW and IW (Fig. 3b, green and pink curves).[28–30] Hence, the stronger HW peaks compared with NHW peaks indicate a higher proportion of HW on the hydrogel surface, predicting the water film is more stable.[31,32] In brief, as shown in Fig. 3c, the 0.5% TE@HNWs surface has a higher intensity ratio of HW ($I_{HW}:I_{NHW}$ = 1.77), which is 15.6% higher than that of the 0.5% TE@flat HNWs surface. The ATR-FTIR results indicate the higher proportion of HW leads to a greater hydrogen-bonding interaction to form a strongly bound and expanded interfacial water network on the TE@HNWs surface.

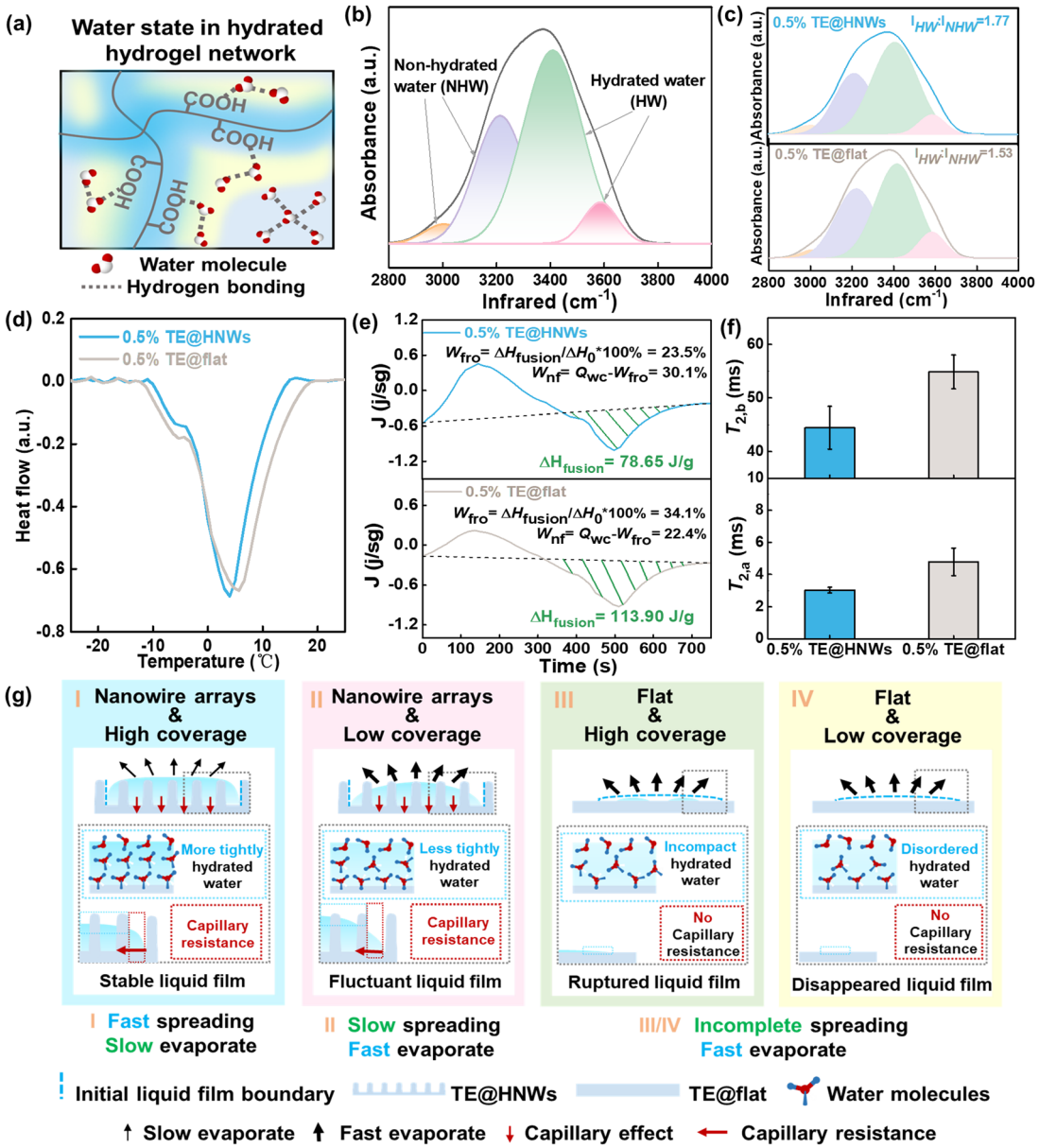

Fig. 3 Hydrated water distribution in different hydrogel surfaces. (a) Schematic of the water in the hydratable hydrogel network, showing strong water/polymer bonding, weakened water/polymer bonding (intermediate water, IW) (yellow area), and normal water/water bonding (free water, FW) (light blue area). (b) ATR-FTIR spectra showing the fitting peaks representing non-hydrated water (NHW, orange and purple curves) and hydrated water (HW, green and pink curves) in the hydrogel networks. (c) Deconvolution of ATR-FTIR spectra of water in 0.5% TE@HNWs and 0.5% TE@flat, and the HW to NHW ratios of 0.5% TE@HNWs and 0.5% TE@flat surface are 1.77 and 1.57. (d) DSC curves of the melting behavior of water frozen in 0.5% TE@HNWs and 0.5% TE@flat surfaces. (e) DSC quantitative analysis of water states in 0.5% TE@HNWs (top) and 0.5% TE@flat (bottom). (f) T_2 values of water in 0.5% TE@HNWs and 0.5% TE@flat surfaces, including $T_{2,b}$ (long time) (top) and $T_{2,a}$ (short time) (bottom). (g) The mechanism of water film stabilization. Error bars are obtained from three parallel samples.

Given that the water in each state shows distinct characteristic phase change behaviors, such as freezing and melting, the hydration state could be further monitored by differential scanning calorimetry (DSC) measurements. It has been demonstrated that BW, which strongly interacts with hydrophilic polymer chains, is non-freezable water. Therefore, there are no endothermic peaks for BW during the measurement. Nevertheless, the IW and FW are freezable, and the main endothermic peak in these curves is categorized as the melting peak of IW and FW.[33,34] There are two peaks located at $\sim -5^{\circ}$ and $\sim 5\ ^{\circ}C$ corresponding to the melting of IW and FW, respectively (Fig. 3d and Fig. S9a, ESI†). In addition, the measured melting peak of 0.5% TE@HNWs is shifted to a lower temperature compared with that of 0.5% TE@flat, which can be interpreted in terms of the supercooling effect based on thermodynamics.[25] These results indicate that more water molecules are hydrated with hydrophilic groups on 0.5% TE@HNWs and the ratio of non-freezable water becomes larger. Furthermore, in order to

quantify the ratio of the state of water, we assume that the enthalpy value ΔH_0 of water in the hydrogel is the same as that of pure water, *i.e.*, 334 J g^{-1}. Then the enthalpy change $\triangle H_{fusion}$ of the endothermic peak can be used to calculate the percentage of frozen water (W_{fro}) and non-frozen water (W_{nf}):

$$W_{fro} = \Delta H_{fusion}/\Delta H_0 \times 100\%$$

$$W_{nf} = Q_{WC} - W_{fro}$$

where ΔH_{fusion} can be calculated from the endothermic peak areas in Fig. 3e. And the water content Q_{wc} of the hydrogel is represented by

$$Q_{WC} = \frac{W}{W_d}$$

where W and W_d are the weights of the water in the fully swollen sample and in the corresponding dried aerogel sample, respectively.[35] According to the fitting results (Fig. 3e), the ratio of W_{nf} to W_{fro} on 0.5% TE@HNWs is higher than that on 0.5% TE@flat. In detail, W_{fro} on 0.5% TE@HNWs is 23.5% and W_{nf} is 30.1%, while W_{fro} on 0.5% TE@flat is 34.1% and W_{nf} is 22.4%. The result proves that the proportion of BW on 0.5% TE@HNWs surface is higher, indicating that the water at this surface is less prone to evaporation, thus promoting the stability of the water film.

To gain further molecular-level insights into the correlation between HW and water film stability, the mobility of the water is assessed by proton spin–spin relaxation time (T_2) measurements on different hydrogel surfaces, as shown in Fig. 3f and Fig. S11b (ESI†). These curves are based on two-component systems, *i.e.*, the bound water protons (labeled ''a'') having a short relaxation time T_2 and the bulk-like protons (labeled ''b'') having a long T_2.[36,37] The hydrophilic group protons and the tightly bound water protons are not included because these are undetectable by the T_2 relaxation measurement due to their extremely short relaxation time.[38] All values of $T_{2,a}$ fluctuate around $\sim$3 ms, showing almost no dependence on the surfaces, whereas the value of $T_{2,b}$ increases substantially from 40 to 50 ms as the surface changes from 0.5% TE@HNWs to 0.5% TE@flat. The larger the value of $T_{2,b}$, the greater is the mobility of hydrated water, which indicates that the mobility of interfacial water molecules is enhanced by the absence of nanowire array structure.

The above results systematically assess the hydrated water state of different hydrogel surfaces. Benefiting from the higher ratio of I_{HW}/I_{NHW} and the lower mobility of water molecules, TE@HNWs exhibit long-term stability of the water film. We speculate that this is mainly due to the introduction of the nanowire arrays to greatly increase the hydrated area of interfacial water compared to flat surfaces. It can be concluded that both nanowire array structure and the hydrophilic layer can strengthen the stability of the water film synergistically.

The mechanism of water film stabilization

Based on water film variability and the hydrated water states on different hydrogel surfaces, the mechanism of water film stabilization is illustrated in Fig. 3g. It mainly involves two key factors: nanowire arrays and hydrophilic layer. When both the nanowire arrays and the high hydrophilic layer coverage are present (Fig. 3g(I)), and the water molecules are strongly trapped in the hydrophilic layer, forming a more tightly hydrated water network. This type of water is characterized by inert chemical activity and a short relaxation time, which inhibits the fluctuation of water molecules and shows a stable state. In addition, owing to the high energy barrier that needs to be overcome for the spontaneous dewetting of water on the nanowire structures, the capillary resistance generated by the nanowire structures further anchors the water film at the initial boundary. Synergistically, the water film exhibits a more stable state. For a lower hydrophilic layer coverage (Fig. 3g(II)), the water molecules on the surfaces are less tightly ordered, causing the water film to fluctuate at an early period. Worse, for the surface without nanowire arrays (Fig. 3g(III) and (IV)), the water molecules in the water film on the flat surface are arranged more incompactly and disordered, and the water film ruptures or even disappears in advance.

It is generally accepted that rapidly spreading surfaces are usually accompanied by unstable rupture of a water film, that is, 'rapid spread, fast evaporation'. These theories hold that a rapidly spreading surface has a larger evaporation area, and the water film at the gas–liquid interface is affected by thermodynamics-dominated evaporation leading to dewetting and rupture. Here, we break with the conventional concept and, inspired by cornea surface, introduce hydrophilic layers and nanostructure *in vitro*, where nanocapillary resistance and a higher proportion of bound water synergically contribute to create a stable water film gel surface with 'rapid spread, slow evaporation' characteristics.

Bionic corneal contact lenses

The optical function of the eye critically depends on the presence of a stable precorneal tear film. As mentioned previously, the TE@HNWs obtained with biomimetic corneal structure and tear composition have composition, hydrophilicity and biocompatibility to match those of an ophthalmic material, and have great potential to be utilized as high-performance continuously wearable contact lenses and artificial cornea. For the practical applications of contact lenses, the TE@HNWs lenses should combine optimal features such as transparency for vision, enough water content to maintain moisture, permeability for oxygen and modulus to ensure eye comfort.[39,40] Furthermore, continuously maintaining water film stability can keep visual resolution.[41] Moreover, to improve the long-term wearing comfortable visual clarity, the lenses should also exhibit an excellent anti-lipid adhesion property (Fig. 4a).

Here, we first characterize and test TE@HNWs lenses in detail as a basic assessment of contact lenses. The results indicate that at the optimal ratio, the lenses have high oxygen permeability, which is a critical requirement for high-performance continuously wearable contact lenses. Besides, water content, transparency, and modulus are comparable to

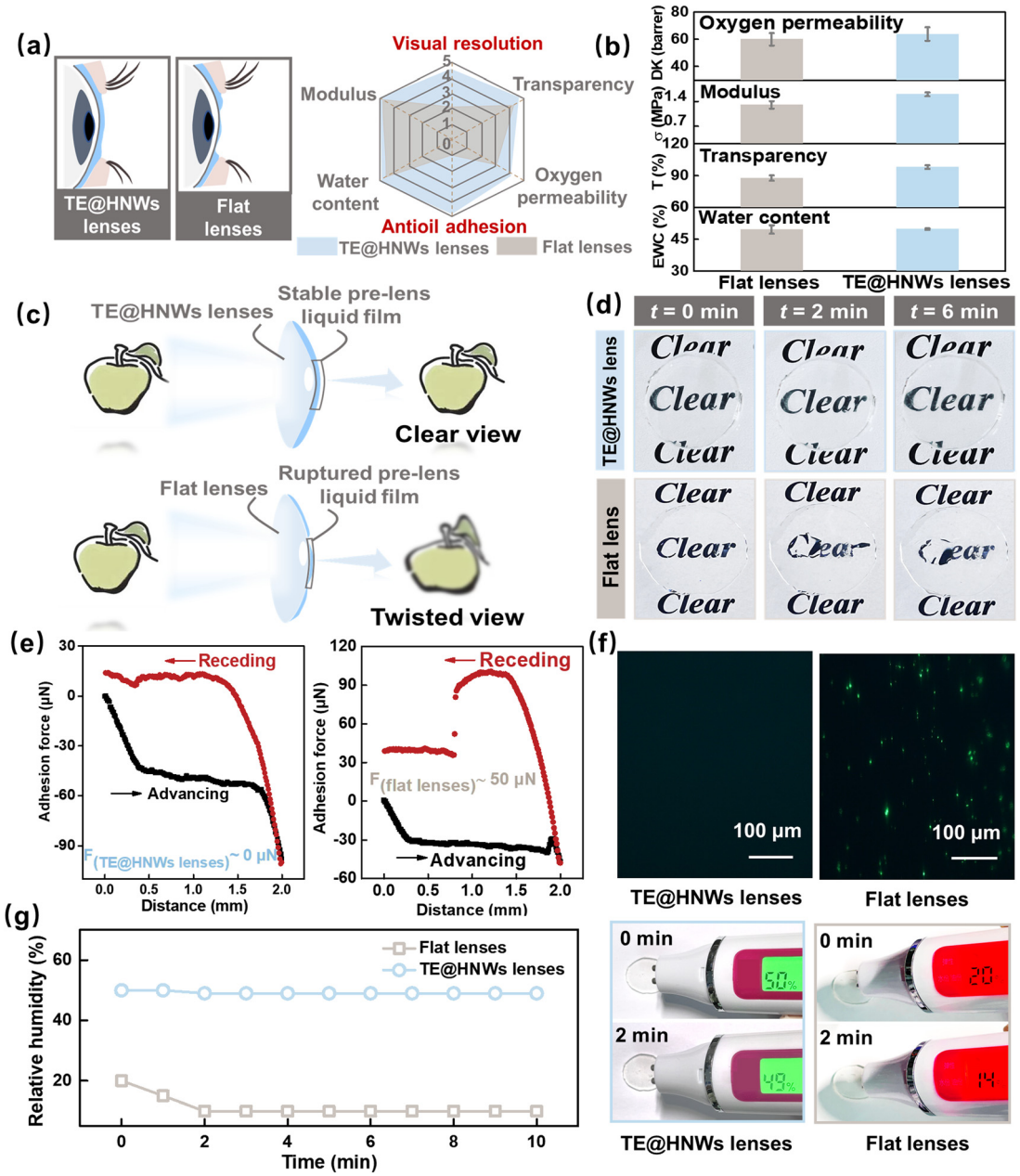

Fig. 4 Incorporation of TE@HNWs into contact lenses as ophthalmic materials. (a) The developed TE@HNWs lenses combine vital advantages, as qualitatively illustrated in a radar chart. (b) Histogram of oxygen permeability, modulus, transparency and water content of flat and TE@HNWs lenses. Error bars are obtained from three parallel samples. (c) TE@HNWs lenses with a stable water film can ensure clear vision, while a rupture and discontinuous water film would make vision distorted and blurred on flat lenses. (d) Representative visual imaging of "Clear" on paper for the TE@HNWs lenses (top row) and the flat lenses (bottom row) captured at different times. (e) Adhesion measurements. Paraffin oil adhesion on the TE@HNWs lenses (left) and flat lenses (right). (f) Representative images of fluorescent-labeled protein (rhodamine-bovine serum albumin) adhered on TE@HNWs lenses (left) and flat lenses (right). (g) Humidity monitoring of the lens surface for 10 minutes and the corresponding optical photograph of the humidity value during 2 minutes which shows the surface humidity changes slowly on TE@HNWs lenses.

those of commercial contact lenses (Fig. 4b and Fig. S10, ESI†). Most importantly, in contrast to the blurry and distorted vision of flat lenses, TE@HNWs lenses can maintain stable and clear vision due to the presence of a non-ruptured water film. (Fig. 4c and d). In addition, the adhesion force result (Fig. 4e) shows that the TE@HNWs lens surface has extremely low adhesion to oil, but for the flat lens surface it is at least 50 μN and with residue remaining on its surface (Fig. S11, ESI†). We speculate that the superoleophobic lens surface can effectively resist the adhesion of lipid substances from tears, ensuring the lenses remain clean and visually clear.[16,42,43] Additionally, the TE@HNWs lenses show remarkable performance in antiprotein adhesion performance (Fig. 4f), effectively reducing the risk of eye infection and increasing the wearing safety.

Furthermore, we monitored the surface humidity for ten minutes and the results show that a flat lens surface is always in a low-humidity range, while the TE@HNWs lenses remain within a high-humidity range, which enable comfortable long-term wear (Fig. 4g). And, the TE@HNWs surface remains robust under long-term blinking friction (Fig. S12, ESI†). Most importantly, TE@HNWs is biocompatible as a contact lens. In detail, the samples are directly cultured on human corneal epithelial cell strain *in vitro* for 24 h, and the absorbance OD value of the cell culture fluid is measured to characterize the cell activity. Higher OD values represent higher cell activity and lower cytotoxicity. In Fig S15 (ESI†), the TE@HNWs lens leads to a high OD value of cell culture fluid, indicating that the lens has superior biocompatibility and no cytotoxicity. These results indicate that the TE@HNWs lenses derived from biomimetic concepts have significant potential as ophthalmic materials in the future.

3. Conclusions

In summary, inspired by the healthy cornea surface, the obtained hybrid TE@HNWs hydrogel is characterized by the dynamic behavior of 'rapid spread, slow evaporation', which could keep long-term wettability and comfort in the air environment, preventing rapid dehydration and evaporation. We clearly clarified that the synergistic effect between capillary resistance of the nanowire arrays and high proportion of HW enhanced the stability of the water film and improved the interfacial humidity. In particular, the nanowire arrays are important initiators for the liquid film stabilization. Furthermore, the higher ratio of I_{HW}/I_{NHW} and the lower mobility of water molecules contribute to a more stable water film. In this work, the nanowire structure and hydrophilic polymer layer are introduced simultaneously, which synergically contributes to long-term moisture retention and water film stability, and provides a new strategy for the development of ophthalmic materials. In addition, this method is simple and easy to operate, which can be expected to be applied to various wearable devices to obtain multi-functional integrated wearable devices with comfort, high hydrophilicity and high humidity.

Author contributions

Y. T. conceived and designed the experiments. Y. F. provided the data of the dry eye disease patients and designed the experiments. P. L. performed the experiments and wrote the original manuscript. P. L., M. Q. and Y. W. revised the manuscript. P. L., Y. W., Y. W., Z. L. and J. Y. discussed and analyzed the data. All authors edited and approved the manuscript.

Data availability

The data supporting this article have been included as part of the ESI.†

Conflicts of interest

There are no conflicts to declare.

Acknowledgements

This research is supported by National Natural Science Foundation (22090052, 21988102, 82271051, 82070926), National Key Research and Development Program of China (2023YFE0203100), Frontier Science Key Projects of CAS (ZDBS-LY-SLH022), Key R&D Project of Shandong Province (2022CXGC010302) and Xiaomi Young Talents Program.

References

1 H. Liu, D. Xu, B. Hu, J. Jiang, M. Li, D. Zhao and W. Zhai, *J. Mater. Chem. A*, 2021, **9**, 4692.
2 Q. He, Y. Cheng, Y. Deng, F. Wen, Y. Lai and H. Li, *Adv. Funct. Mater.*, 2023, **34**, 2308974.
3 W. Zhao, F. Shao, F. Sun, Z. Su, S. Liu, T. Zhang, M. Zhu, Z. Liu and X. Zhou, *Adv. Mater.*, 2023, **35**, e2300876.
4 K. Zhao, Y. Zhao, R. Qian and C. Ye, *Chem. Eng. J.*, 2023, **477**, 147109.
5 A. Q. Khan, K. Yu, J. Li, X. Leng, M. Wang, X. Zhang, B. An, B. Fei, W. Wei, H. Zhuang, M. Shafiq, L. Bao, Z. Liu and X. Zhou, *Adv. Fiber. Mater.*, 2022, **4**, 1572.
6 Y. Lu, G. Yang, S. Wang, Y. Zhang, Y. Jian, L. He, T. Yu, H. Luo, D. Kong, Y. Xianyu, B. Liang, T. Liu, X. Ouyang, J. Yu, X. Hu, H. Yang, Z. Gu, W. Huang and K. Xu, *Nat. Electron.*, 2024, **7**, 51.
7 Y. Mu, W. Yang, J. Cheng, L. Lin, L. Lin, L. Li, N. Jin, C. Liu and L. Dong, *IEEE Sens. J.*, 2022, **22**, 7816.
8 Y. Niu, H. Liu, R. He, M. Luo, M. Shu and F. Xu, *Small*, 2021, **17**, e2101151.
9 H. Liu, M. Li, C. Ouyang, T. J. Lu, F. Li and F. Xu, *Small*, 2018, **14**, e1801711.
10 A. Sharma and E. Ruckenstein, *J. Colloid Interface Sci.*, 1984, **106**, 12–27.
11 R. J. Braun, *Annu. Rev. Fluid Mech.*, 2012, **44**, 267.
12 F. J. Holly and M. A. Lemp, *Exp. Eye Res.*, 1971, **11**, 239–250.
13 A. P. Corfield, *Bba. Rev. Cancer*, 1850, **2015**, 236.
14 P. A. Eso and I. K. Gipson, *Exp. Eye Res.*, 2001, **73**, 281–289.
15 M. Matsuzawa, T. Ando, S. Fukase, M. Kimura, Y. Kume, T. Ide, K. Izawa, A. Kaitani, M. Hara, E. Nakamura, A. Kamei, A. Matsuda, N. Nakano, K. Maeda, N. Tada, H. Ogawa, K. Okumura, A. Murakami, N. Ebihara and J. Kitaura, *Nat. Commun.*, 2023, **14**, 1417.
16 Y. Zhu, R. Nasiri, E. Davoodi, S. Zhang, S. Saha, M. Linn, L. Jiang, R. Haghniaz, M. C. Hartel, V. Jucaud, M. R. Dokmeci, A. Herland, E. Toyserkani and A. Khademhosseini, *Small*, 2023, **19**, e2207017.
17 S. Kusama, K. Sato, S. Yoshida and M. Nishizawa, *Adv. Mater. Technol.*, 2020, **5**, 1900889.
18 M. Puertas-Bartolome, I. Gutierrez-Urrutia, L. L. Teruel-Enrico, C. N. Duong, K. Desai, S. Trujillo, C. Wittmann and A. Del Campo, *Adv. Mater.*, 2024, **36**, e2313848.

19 R. T. Arwani, S. C. L. Tan, A. Sundarapandi, W. P. Goh, Y. Liu, F. Y. Leong, W. Yang, X. T. Zheng, Y. Yu, C. Jiang, Y. C. Ang, L. Kong, S. L. Teo, P. Chen, X. Su, H. Li, Z. Liu, X. Chen, L. Yang and Y. Liu, *Nat. Mater.*, 2024, **23**, 1115.
20 W. Miao, S. Zheng, J. Zhou, B. Zhang, R. Fang, D. Hao, L. Sun, D. Wang, Z. Zhu, X. Jin, Y. Tian and L. Jiang, *Adv. Mater.*, 2021, **33**, e2007152.
21 C. A. Rickert, B. Wittmann, R. Fromme and O. Lieleg, *ACS Appl. Mater. Interfaces*, 2020, **12**, 28024–28033.
22 B. Winkeljann, M. G. Bauer, M. Marczynski, T. Rauh, S. A. Sieber and O. Lieleg, *Adv. Mater. Interfaces*, 2020, **7**, 1–12.
23 W. Chen, Q. Wang, J. Chen, Q. Zhang, X. Zhao, Y. Qian, C. Zhu, L. Yang, Y. Zhao, X. Y. Kong, B. Lu, L. Jiang and L. Wen, *Nano Lett.*, 2020, **20**, 5705–5713.
24 Y. Guo, H. Lu, F. Zhao, X. Zhou, W. Shi and G. Yu, *Adv. Mater.*, 2020, **32**, 1–8.
25 T. Nakaoki and H. Yamashita, *J. Mol. Struct.*, 2008, **875**, 282–287.
26 X. Zhou, Y. Guo, F. Zhao, W. Shi and G. Yu, *Adv. Mater.*, 2020, **32**, 1–7.
27 Y. Guo, H. Lu, F. Zhao, X. Zhou, W. Shi and G. Yu, *Sci. Adv.*, 2019, **5**, 1–7.
28 D. F. Liu, G. Ma, L. M. Levering and H. C. Allen, *J. Phys. Chem. B*, 2004, **108**, 2252–2260.
29 N. Li, Z. Xu, S. Zheng, H. Dai, L. Wang, Y. Tian, Z. Dong and L. Jiang, *Adv. Mater.*, 2021, **33**, e2003559.
30 W. Guo, J. Chen, S. Sun and Q. Zhou, *J. Mol. Struct.*, 2018, **1171**, 600.
31 Y. Guo and G. Yu, *Account Mater. Res.*, 2021, **2**, 374.
32 Y. Guo, X. Zhao, F. Zhao, Z. Jiao, X. Zhou and G. Yu, *Energy Environ. Sci.*, 2020, **13**, 2087.
33 W. G. Liu and K. D. Yao, *Polymer*, 2001, **42**, 3943–3947.
34 W. Li, F. Xue and R. Cheng, *Polymer*, 2005, **46**, 12026.
35 L. Rui, W. Liang, Y. Q. Zhang, H. L. Zhang, B. Zhang, B. L. Huang and Y. M. Wei, *Trans. Chin. Soc. Agric. Eng.*, 2015, **31**, 288–294.
36 S. W. Wu, Z. Y. He, J. G. Zang, S. L. Jin, Z. W. Wang, J. P. Wang, Y. F. Yao and J. J. Wang, *Sci. Adv.*, 2019, **5**, 1–6.
37 Z. Y. He, W. J. Xie, Z. Q. Liu, G. M. Liu, Z. W. Wang, Y. Q. Gao and J. J. Wang, *Sci. Adv.*, 2016, **2**, 1–7.
38 P. McConville and J. M. Pope, *Polymer*, 2001, **42**, 3559–3568.
39 P. Chaudhari, V. M. Ghate and S. A. Lewis, *Eur. J. Pharm. Biopharm.*, 2021, **161**, 80.
40 L. Bengani and A. Chauhan, *Future Med. Chem.*, 2012, **4**(17), 2141–2143.
41 N. Keir and L. Jones, *Eye Contact. Lens*, 2013, **39**, 100–108.
42 J. Seo, W. Y. Byun, F. Alisafaei, A. Georgescu, Y. S. Yi, M. Massaro-Giordano, V. B. Shenoy, V. Lee, V. Y. Bunya, D. Huh, J. Seo, W. Y. Byun, F. Alisafaei, A. Georgescu, Y. S. Yi, M. Massaro-Giordano, V. B. Shenoy, V. Lee, V. Y. Bunya and D. Huh, *Nat. Med.*, 2019, **25**, 1310–1318.
43 J. Pan, W. Zhang, J. Zhu, J. Tan, Y. Huang, K. Mo, Y. Tong, Z. Xie, Y. Ke, H. Zheng, H. Ouyang, X. Shi and L. Gao, *Adv. Mater.*, 2023, **35**, e2207750.

